PV-based off-board electric vehicle battery charger using BIDC

Ankita PAUL, Krithiga SUBRAMANIAN*, **Sujitha NACHINARKINIYAN**®

School of Electrical Engineering, Vellore Institute of Technology, Chennai Campus, Chennai, Tamil Nadu, India

Abstract: In recent years, the use of renewable energy sources is increasing drastically in several sectors, which leads to its role in the automobile industry to charge electric vehicle (EV) batteries. In this paper, a photovoltaic (PV) array-fed off-board battery charging system using a bidirectional interleaved DC-DC converter (BIDC) is proposed for light-weight EVs. This off-board charging system is capable of operating in dual mode, thereby supplying power to the EV battery from the PV array in standstill conditions and driving the DC load by the EV battery during running conditions. This dual mode operation is accomplished by the use of a three-phase BIDC. The model of the proposed system is simulated in MATLAB/Simulink software while a hardware prototype of 250 W is fabricated and tested in the laboratory. Simulation and experimental results are furnished in this paper.

Key words: Electric vehicle, photovoltaic array, battery, bidirectional DC-DC charger

1. Introduction

Ever-growing stress on fossil fuels has led to the depletion of nonrenewable sources of energy and also damaged the environment. This increases the need for clean and abundantly available sources of renewable energy. Among the available renewable sources, solar and wind energy are widely preferred. With advancement in technology, these energy sources were tapped to convert energy into a more useful form of energy, which is electricity. Research in this field enabled the integration of these renewable energy sources with power electronic converters for various applications [1,2].

Environmental concerns owing to the generation of greenhouse gases by conventional internal combustion (IC) engines have also paved the way for the growth of electric vehicles (EV). EVs have found their place in the global market because they do not emit pollutants to the environment and have the inherent quality of being quiet [3–5]. Initially, these vehicles found applications inside buildings, in warehouses, and on golf courses, where pollution is to be controlled. EVs are also used as mobility devices for the elderly and disabled. EVs are now employed for regular transportation purposes, also. Hence, PV array power is utilized for charging EV batteries with the help of advanced power converter topologies [6,7].

The evolution of EV batteries started with lead acid batteries, after which it moved on to nickel and most recently lithium batteries [8]. Since lead acid batteries have low chemical leakage, specific energy, and poor temperature characteristics, modern EVs do not use lead acid batteries and those have been replaced by lithium ion batteries. They are more preferred due to higher power density, high efficiency, compact size, and light weight [9,10]. These batteries require accurate control of voltage during charging conditions. Moreover, these batteries have fast charging capacity, wide operating temperature range, long life cycle, and low self-discharge

---

*Correspondence: s_krithiga@yahoo.com

rate. In addition to these advantages, if these batteries are accidentally overcharged or short-circuited, they have low risk of explosion. This makes the lithium ion battery most suitable for EVs.

EV battery chargers can be broadly classified as on-board chargers and off-board chargers. On-board chargers are installed on the vehicle and off-board chargers are installed outside of the vehicle. Various power electronic converters are used for charging EV batteries. Among various power converters, multiport converters (MPCs) are popular in hybrid electric vehicles (HEVs) due to their capability of interfacing power sources and energy storage elements like PV arrays, ultracapacitors, supercapacitors, fuel cells, and batteries with the loads in EVs like the motor, lights, power windows and doors, radios, amplifiers, and mobile phone chargers. These multiport converters are classified as isolated and nonisolated converters. Various unidirectional and bidirectional isolated and nonisolated MPCs are reviewed in the literature [11–16]. An isolated MPC uses a transformer core for isolation, which increases the cost and weight of the EV. Also, the number of active switches is high, increasing the complexity of control circuitry. Nonisolated MPCs are classified into topology with shared components between the converters and topology with converters connected in parallel. The advantages of nonisolated MPCs are the simple and compact structure with lower component count and low cost. However, voltage levels between the ports are not flexible and achieving ZVS switching is complex in these MPCs [14].

For light-weight EV off-board charging systems like electric bikes, the EV battery is used to drive the EV motor in moving conditions, and in standstill conditions, the EV battery is charged using the renewable energy sources available in the charging station or parking lot. The advantages of off-board chargers over on-board chargers are higher power transfer, lower maintenance cost, higher energy transfer rate, simple energy management strategy, and reduced weight of the EV [17]. Hence, simple bidirectional converters are more suitable for the off-board light-weight EV chargers compared to MPCs, as there is no need for multiport converters in these applications. Also, bidirectional converters have the advantages of fewer active components, flexible power flow, and reduced size. These bidirectional converters are also classified as nonisolated and isolated converters. In an isolated bidirectional DC-DC converter, the isolation is usually provided by a transformer. The circuit operation of such converters brings the usage of leakage inductance of the transformer as the main energy storing and transferring element to deliver bidirectional power [18–20]. However, the addition of a transformer leads to increased losses and price, whereas nonisolated bidirectional converters are best suited for these light-weight EV applications [21–23].

A nonisolated bidirectional DC-DC converter is typically a combination of a boost and a buck type converter. The circuit is operated in discontinuous conduction mode (DCM) and with minimized inductance value in order to improve the efficiency. The operation in DCM introduces high ripple current, which is reduced by implementing the multiple phase interleaving technique. Another advantage of DCM operation is that it minimizes turn-on losses. However, it increases the turn-off losses, which largely affect the efficiency of the converter and also cause parasitic ringing effect in inductor current.

The turn-off loss is reduced by using a snubber capacitor across the switch, which is discharged before the switch is turned on. This is accomplished by a soft switching technique, which is employed during both turn-on and turn-off periods. This soft switching scheme is considered as a zero voltage resonant transition (ZVRT) switching technique, which helps in minimizing the inductor current parasitic ringing effect. Thus, the resonant soft switching technique can be implemented in power stages to improve the efficiency of the nonisolated bidirectional DC-DC converter [24–27].

Therefore, in this paper, a PV array is integrated with a bidirectional DC-DC converter for charging the battery of an EV. The bidirectional converter used in the proposed system is operated in both forward and
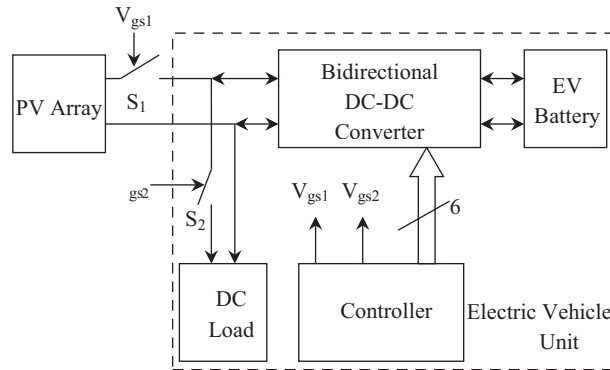
Figure 1. Block diagram of the proposed system.

reverse directions in boost and buck modes, respectively. This helps to charge the EV battery from the PV array in a forward direction and discharge the EV battery in a reverse direction to drive the DC load.

2. Description of the proposed system

The proposed off-board charging system consists of a PV array, a half-bridge BIDC, an EV battery, a controller, and a DC load as shown in Figure 1. In this system, the BIDC, battery, controller, and DC load are present in the EV unit while the PV array is located in the charging station. The controller is used to generate the gate pulses to the BIDC for the flow of power in both directions accordingly. Also, the controller generates the gate pulses to switches S_1 and S_2 to isolate the PV array and DC load from the system, respectively. The proposed system operates in two modes: forward and reverse mode, as explained in this section.

2.1. Forward mode

The BIDC operates in boost mode in the forward direction. In this mode, switch S_1 is always on while switch S_2 is always off, thereby disconnecting the DC load from the system. The PV array converts the solar energy into usable power and supplies the power to the BIDC, which boosts the PV array voltage to charge the EV battery. In this mode, the EV is in standstill position and its battery is charged in the charging station. This mode is also referred to as battery-charging mode.

2.2. Reverse mode

The BIDC operates in buck mode in the reverse direction. In this mode, switch S_1 is always off, while switch S_2 is always on. Thus, the PV array is disconnected from the EV unit and the DC load gets connected to the BIDC. In this mode, the battery discharges through the BIDC, supplying power to the DC load. In this mode, the EV is in running condition and is disconnected from the charging station. In the running condition, the discharging battery power drives the DC load, which can be either the DC motor or other DC loads inside the EV itself. This mode is also referred to as battery-discharging mode.

3. Operation of bidirectional interleaved DC-DC converter

The circuit topology of the half-bridge bidirectional interleaved DC-DC converter employed in the proposed system is shown in Figure 2. The EV battery and PV array are located on the high voltage side and on the low voltage side of the converter, respectively. Switches S_{L1}, S_{L2}, and S_{L3} act as the active switches in boost mode, whereas in buck mode, switches S_{U1}, S_{U2}, and S_{U3} are active. Each of these switches has their own antiparallel

diode and parallel snubber capacitor. In the proposed system, a ZVRT switching strategy has been employed for implementing a soft switching technique. The inductors L_1, L_2, and L_3 act as boost inductors when the converter is operating in boost mode and act as low-pass filters when the converter operates in buck mode. The capacitors C_L and C_H act as smoothing energy buffer elements. The ripple current passing through these capacitors is minimized by the interleaved inductor currents.

Each leg of BIDC comprises two switches, whose gate pulses are 180° phase shifted from each other. In boost mode, the gate pulses are fed to the switches of leg 1 at 0° phase and the pulses to leg 2 switches are 120° phase shifted with respect to that of leg 1 switches and the leg 3 pulses are phase shifted from that of leg 2 and leg 1 switches by 120° and 240°, respectively. In buck mode, the gate pulses are fed to the leg 3 switches with 0° phase and the leg 2 and leg 1 pulses are 120° and 240° phase shifted with respect to that of leg 3 switches, respectively. The modes of operation of the converter are analyzed by considering the operation of a single leg, as explained in this section [24].

3.1. Boost mode (forward mode)

The detailed explanation on operation of the BIDC in boost mode is as follows:

Mode 1: This mode begins when switch S_{L1} is turned on and S_{U1} is turned off. The battery gets charged by the capacitor voltage, C_H. In this mode, switch S_{L1} is on and carries inductor current, I_{L1}, as shown in Figure 3a. In this mode, voltage across switch S_{L1} becomes zero and the initial positive inductor current, I_{L1}, is then transferred swiftly to the snubber capacitor.

Mode 2: Mode 2 is the dead time period. During this period, all the switches are off, as shown in Figure 3b, and C_{U1} discharges to charge the capacitor, C_H, and the battery. The snubber capacitors, C_{L1}, connected in parallel to switch S_{L1}, start to charge by the inductor current, I_{L1}, and voltage across S_{L1} starts increasing until the antiparallel diode, D_{U1}, across the upper switch, S_{U1}, is forward biased.

Mode 3: In this mode also, all the switches are off, as shown in Figure 3c, and the voltage across switch S_{L1} is high. The inductor current, I_{L1}, freewheels through the diode, D_{U1}, forward biasing it, and makes the voltage across switch S_{U1} to be zero.
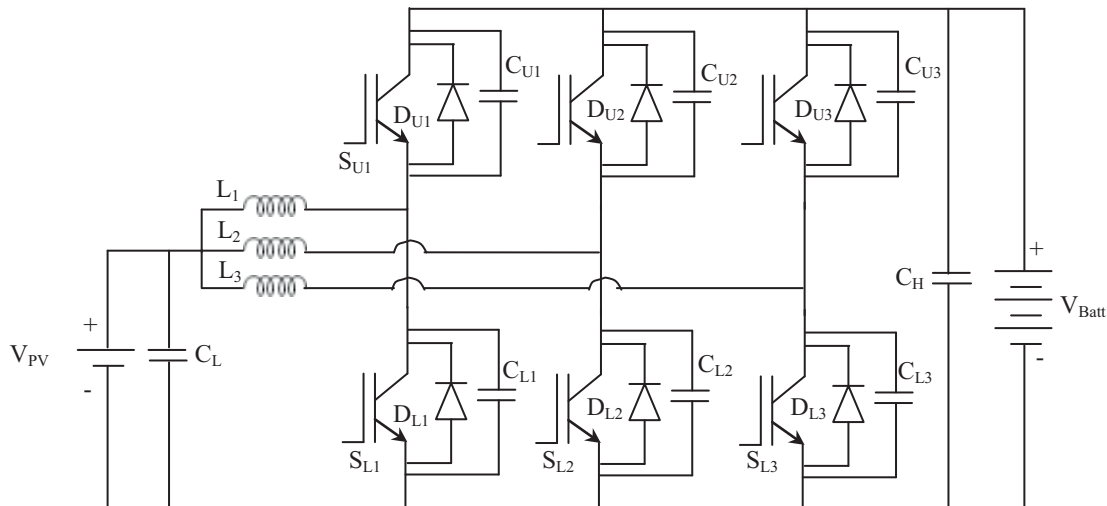

Figure 2. Schematic diagram of half-bridge bidirectional interleaved DC-DC converter.
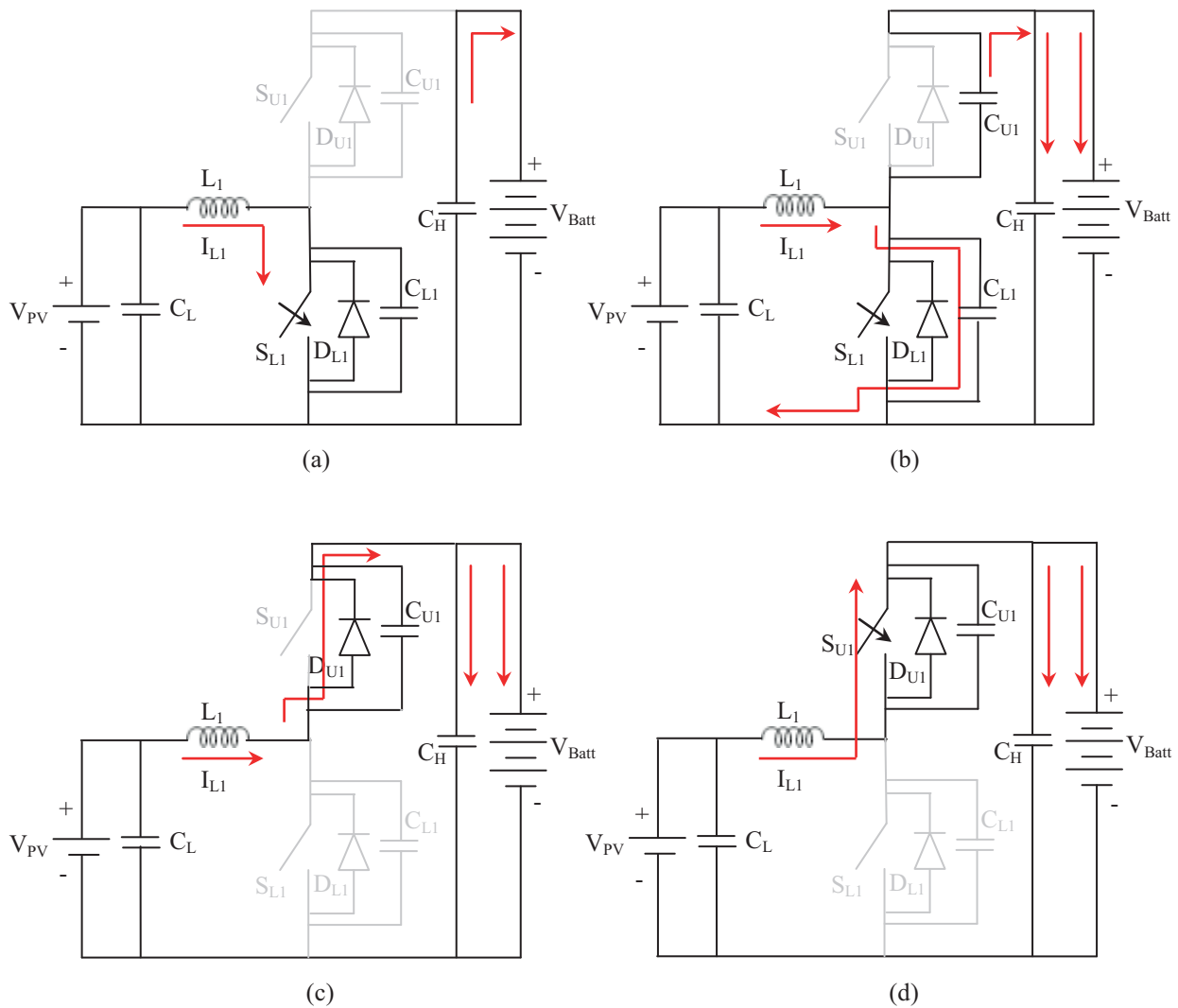
Mode 4: In this mode, switch S_{U1} is turned on at zero voltage with S_{L1} being turned off, as shown in Figure 3d. The ZVRT switching is identical during the process of flow of commutating current from S_{U1} to S_{L1}, except that the inductor current is of opposite polarity during the switching interval.

3.2. Buck mode (reverse mode)

The operation of the BIDC in buck mode is explained in this section for 4 different modes.

Mode 1: Mode 1 begins when the gate signal turns on switch S_{U3}. The battery discharges through S_{U3} and L_3 to load, as shown in Figure 4a.

Mode 2: Mode 2 is the dead time period. During this mode, all the switches are in the off-state, as shown in Figure 4b. The battery discharges through C_{U3} and L_3 to load, thereby charging the snubber capacitor, C_{U3}, and the capacitor, C_{L3} is discharging in this mode. The voltage across the upper switch, S_{U3}, increases, until the antiparallel diode, D_{L3}, across the lower switch, S_{L3}, is forward biased.

Figure 3. Modes of operation of the bidirectional converter in boost mode: a) mode 1, b) mode 2, c) mode 3, and d) mode 4.

Mode 3: In this mode, all the switches are off, and as the voltage across switch S_{U3} is high, the inductor current, I_{L3}, freewheels through the diode, D_{L3}, which makes the voltage across switch S_{L3} be zero, as shown in Figure 4c.

Mode 4: In this mode, S_{L3} is turned on at zero voltage with upper switch S_{U3} being turned off, as shown in Figure 4d. The ZVRT switching is identical during the process of flow of commutating current from S_{L3} to S_{U3}, except that the inductor current is of opposite polarity during the switching interval.

4. Design of the proposed system

The inductor in the BIDC plays a significant role in the system performances, as follows: materialization of complimentary control ZVRT switching, switching losses, and converter size. Thus, optimization of the inductor values with all the other design considerations is necessary.

In boost mode, the relationship between battery current I_{Batt}, inductor peak current I_{Peak}, minimum
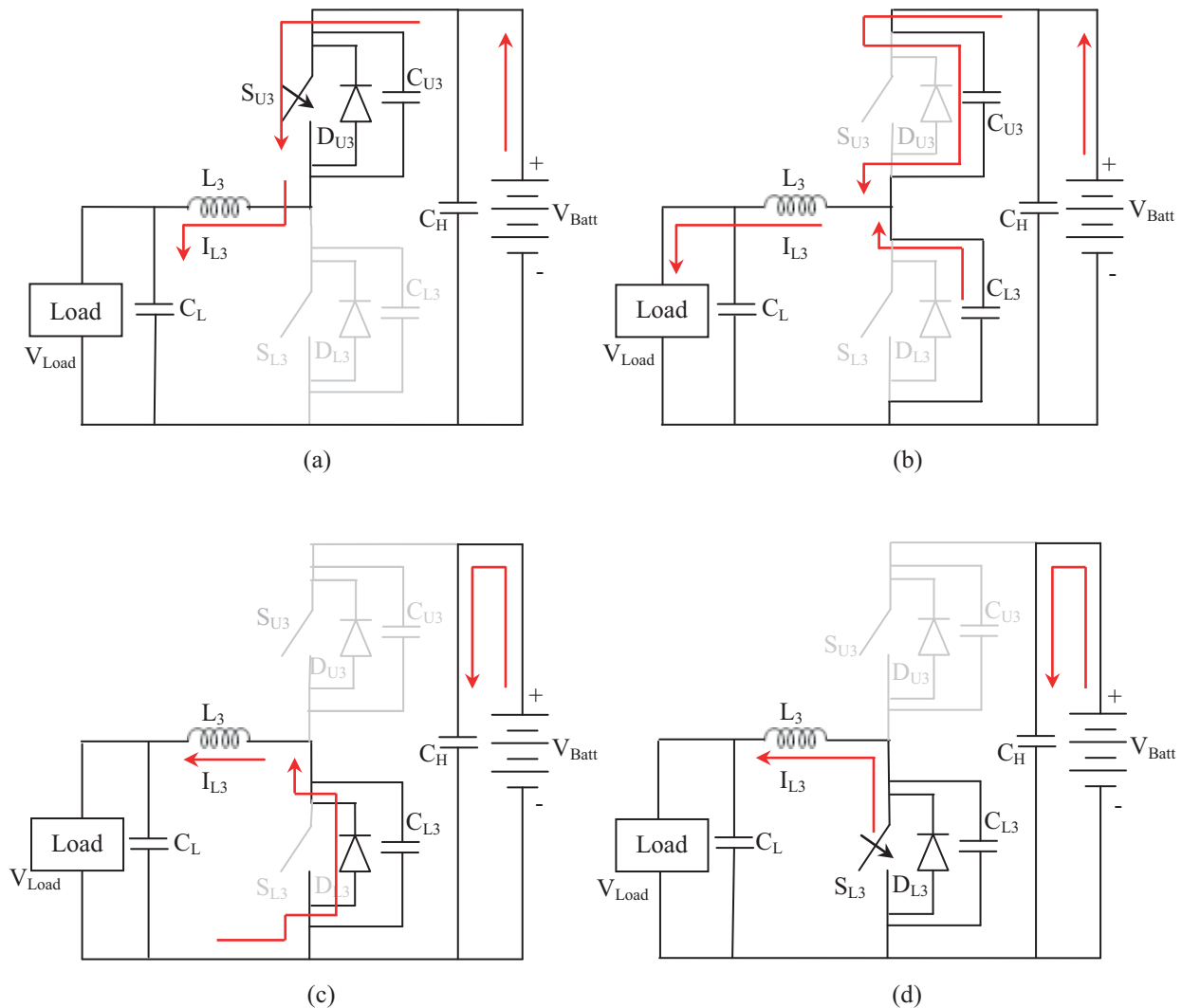
Figure 4. Modes of operation of the bidirectional converter in buck mode: a) mode 1, b) mode 2, c) mode 3, and d) mode 4.

inductor current I_{min}, and average inductor current I_{avg} is expressed by Eqs. (1)–(4) [24]:

$$I_{batt} = \frac{P}{V_{batt}}, \tag{1}$$

$$I_{Peak} = I_{batt} + \Delta I, \tag{2}$$

$$I_{min} = I_{batt} - \Delta I, \tag{3}$$

$$I_{avg} = \sqrt{I_{batt}^2 + \frac{\Delta I^2}{3}}. \tag{4}$$

The voltage conversion ratio in boost mode is given by the following equation:

$$\frac{V_{batt}}{V_{PV}} = \frac{1}{1 - D_{Boost}}, \tag{5}$$

where P is the battery power,

$\quad$ V_{batt} is the EV battery voltage,

$\quad$ V_{PV} is the PV module voltage,

$\quad$ ΔI is the inductor ripple current, and

$\quad$ D_{Boost} is the boost mode duty cycle.

As explained in Section 3.1, it is evident that the realization of ZVRT gate signal generation is possible only when a small portion of the inductor current is negative. This feature can only be acquired by limiting the inductance value below the critical inductance, L_{cric}, as expressed in Eq. (6):

$$L_{cric} = \frac{3V_{Batt}^2 D_{Boost}(1 - D_{Boost})^2}{2Pf_s}, \tag{6}$$

where f_s is the switching frequency.

The inductor ripple current, ΔI, and the capacitance value, C_H, on the high voltage side of the BIDC are given by the following equations:

$$\Delta I = \frac{V_{PV}(V_{Batt} - V_{PV})}{V_{Batt} f_s L}, \tag{7}$$

$$C_H = \frac{D_{Boost}P}{2f_s V_{Batt}^2}. \tag{8}$$

For operation of the BIDC in buck mode, the relationship between load current I_{Load}, inductor peak current I_{Peak}, minimum inductor current I_{min}, and average inductor current I_{avg} is expressed in Eqs. (9)–(12) and the voltage conversion ratio is given by Eq. (13) [24]:

$$I_{Load} = \frac{P}{V_{Load}}, \tag{9}$$

$$I_{Peak} = I_{Load} + \Delta I, \tag{10}$$

$$I_{min} = I_{Load} - \Delta I, \tag{11}$$

$$I_{avg} = \sqrt{I_{Load}^2 + \frac{\Delta I^2}{3}}, \tag{12}$$

$$\frac{V_{load}}{V_{Batt}} = D_{Buck}, \tag{13}$$

where P is the DC load power,

V$_{Load}$ is the DC load voltage, and

D$_{Buck}$ is the buck mode duty cycle.

As explained for boost mode, the value of inductance should be below the critical value in this mode also. The critical inductance, L$_{cric}$, in this mode is expressed as:

$$L_{cric} = \frac{3V_{Load}^2(1 - D_{Buck})}{2Pf_s}. \tag{14}$$

The inductor ripple current, ΔI, and the capacitance, C$_L$, on the low voltage side are given by the following equations:

$$\Delta I = \frac{V_{Batt}(V_{Batt} - V_{load})}{2V_{Batt}f_sL}, \tag{15}$$

$$C_L = \frac{V_{Batt}D_{Buck}(1 - D_{Buck})}{8f_s^2L\Delta V_c}. \tag{16}$$

Based on Eqs. (6), (8), (14), and (16), the values of inductors and capacitors on high voltage and low voltage sides of the BIDC are designed.

5. Simulation studies and results

MATLAB/Simulink software is used for the simulation studies of the proposed system. The PV module is modeled using its classical equation [28]. The proposed BIDC converter is modeled using power MOSFETs, inductors, and capacitors available in the SimPowerSystems Blockset in the Simulink library. The PV module model is integrated with the developed BIDC model along with the battery model available in the Simulink library for developing the proposed system as shown in Figure 5. Additionally, two switches, S$_1$ and S$_2$, are used in the model for isolating the PV module and DC load in buck and boost mode, respectively. The simulation parameters are provided in Table 1.

The simulation of the proposed system was carried out in both boost and buck mode separately and the results are furnished along with experimental results in Section 6. Also, the dynamic response of the system was investigated using the developed simulation model.

Simulation results showing the dynamic response of the system are depicted in Figure 6. Waveforms of PV module voltage, V$_{PV}$, and current, I$_{PV}$, are shown in Figure 6a and Figure 6b. In boost mode, switch S$_1$ is
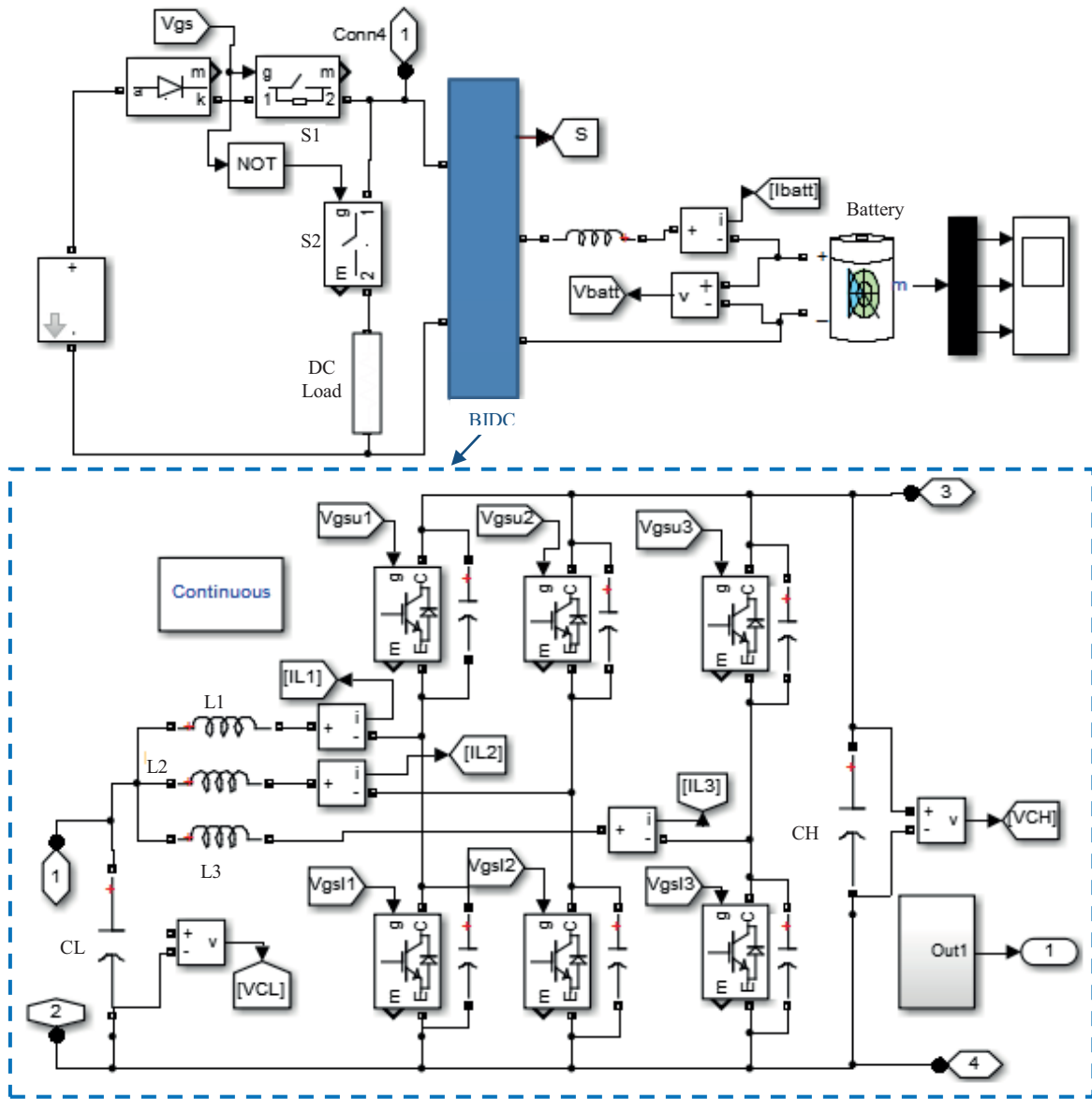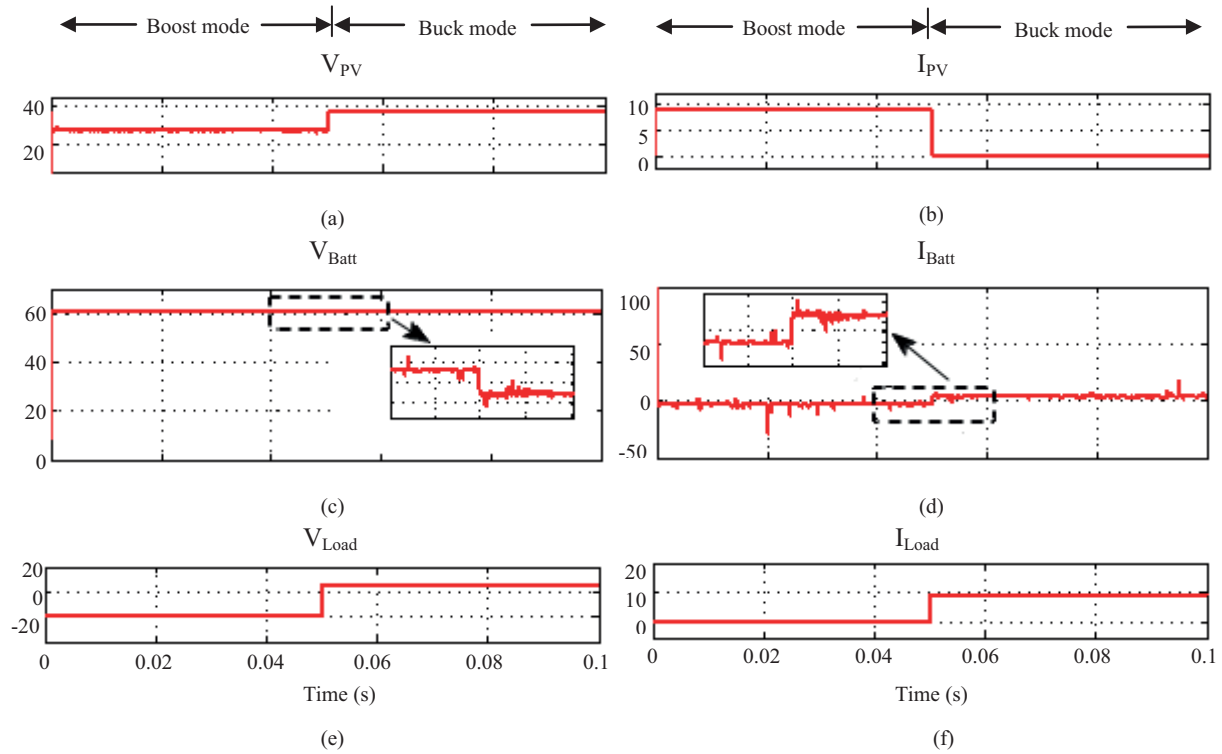
Figure 5. Simulation diagram of the proposed system.

Table 1. Simulation parameters.

Parameters	Values
PV module open circuit voltage, V_{OC}	$37.25V$
PV module short circuit current, I_{SC}	$8.75A$
Maximum PV module Power, P_{PV}	$250W$
Nominal Battery voltage, V_{PV}	$60V$
Battery capacity	$6Ah$

Figure 6. Waveforms of (a) PV module voltage, V_{PV}; (b) PV module current, I_{PV}; (c) EV battery voltage, V_{Batt}; (d) EV battery current, I_{Batt}; (e) load voltage, V_{Load}; and (f) load current, I_{Load}.
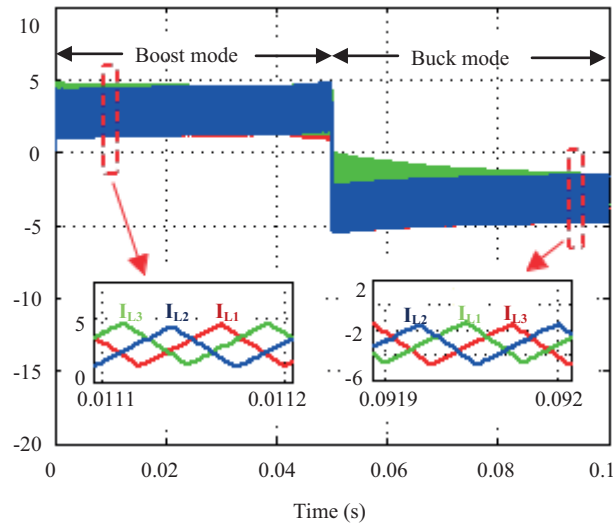
Figure 7. Inductor current waveforms.

ON and switch S_2 is OFF, and a PV module of 250 W is connected to the BIDC with DC load being isolated from the system. In this mode, PV module voltage V_{PV} of 27.68 V is boosted to 60 V to charge the EV battery as depicted in Figure 6c. The charging mode of the EV battery is indicated by the negative battery current, I_{Batt}, as shown in Figure 6d. Furthermore, the DC load voltage, V_{Load}, shown as zero in Figure 6e, indicates that the DC load is isolated from the system.
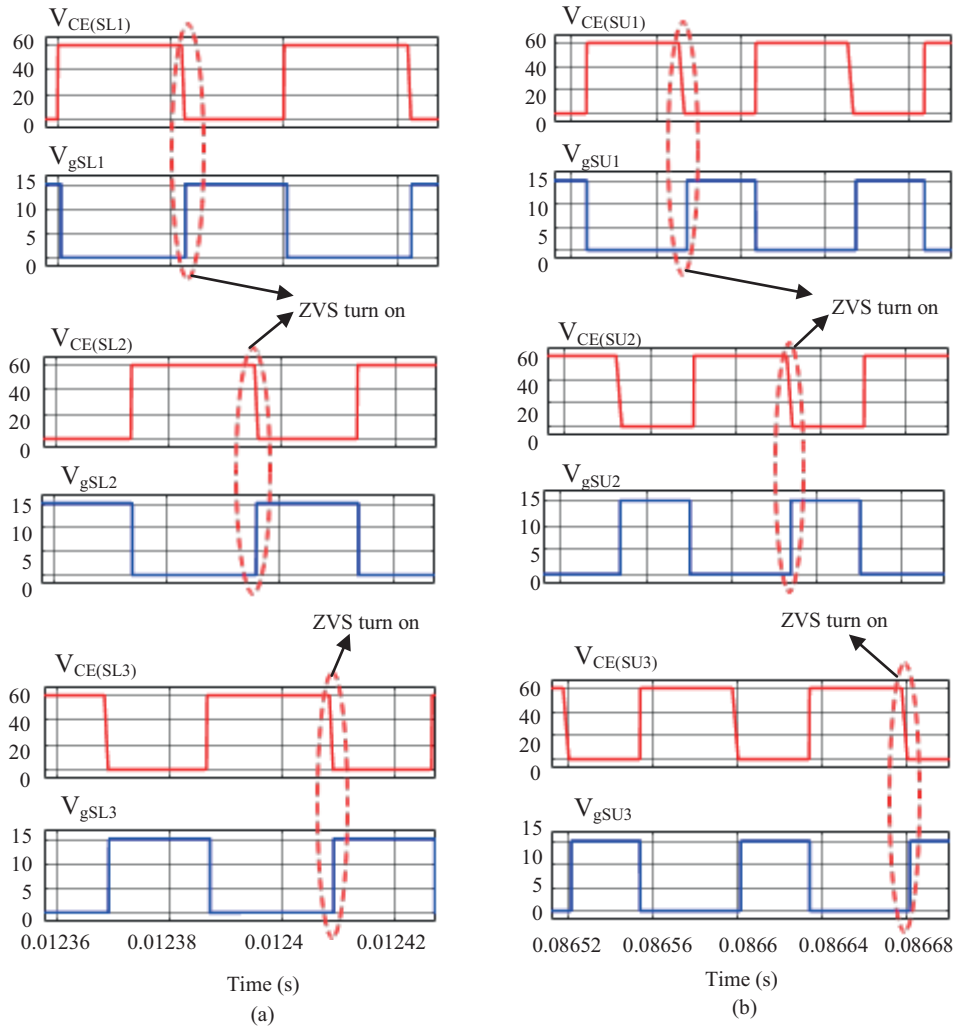
Figure 8. Zero voltage switching waveforms of (a) lower switches in boost mode and (b) upper switches in buck mode.
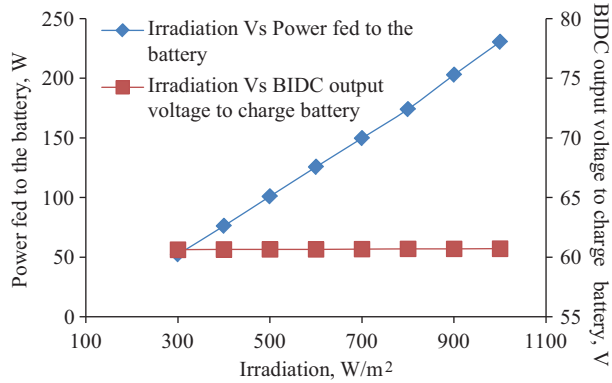

Figure 9. Characteristics of the proposed system with change in PV module irradiation conditions in boost mode.
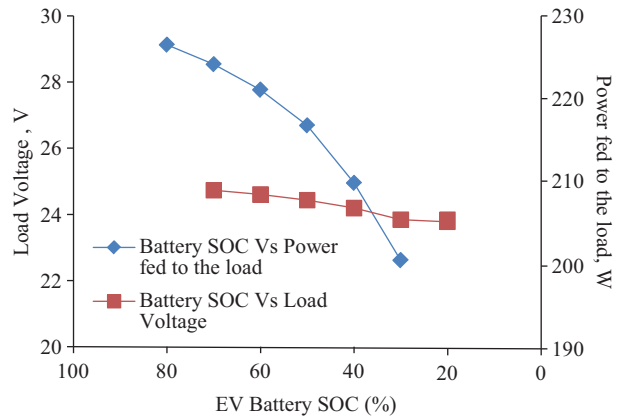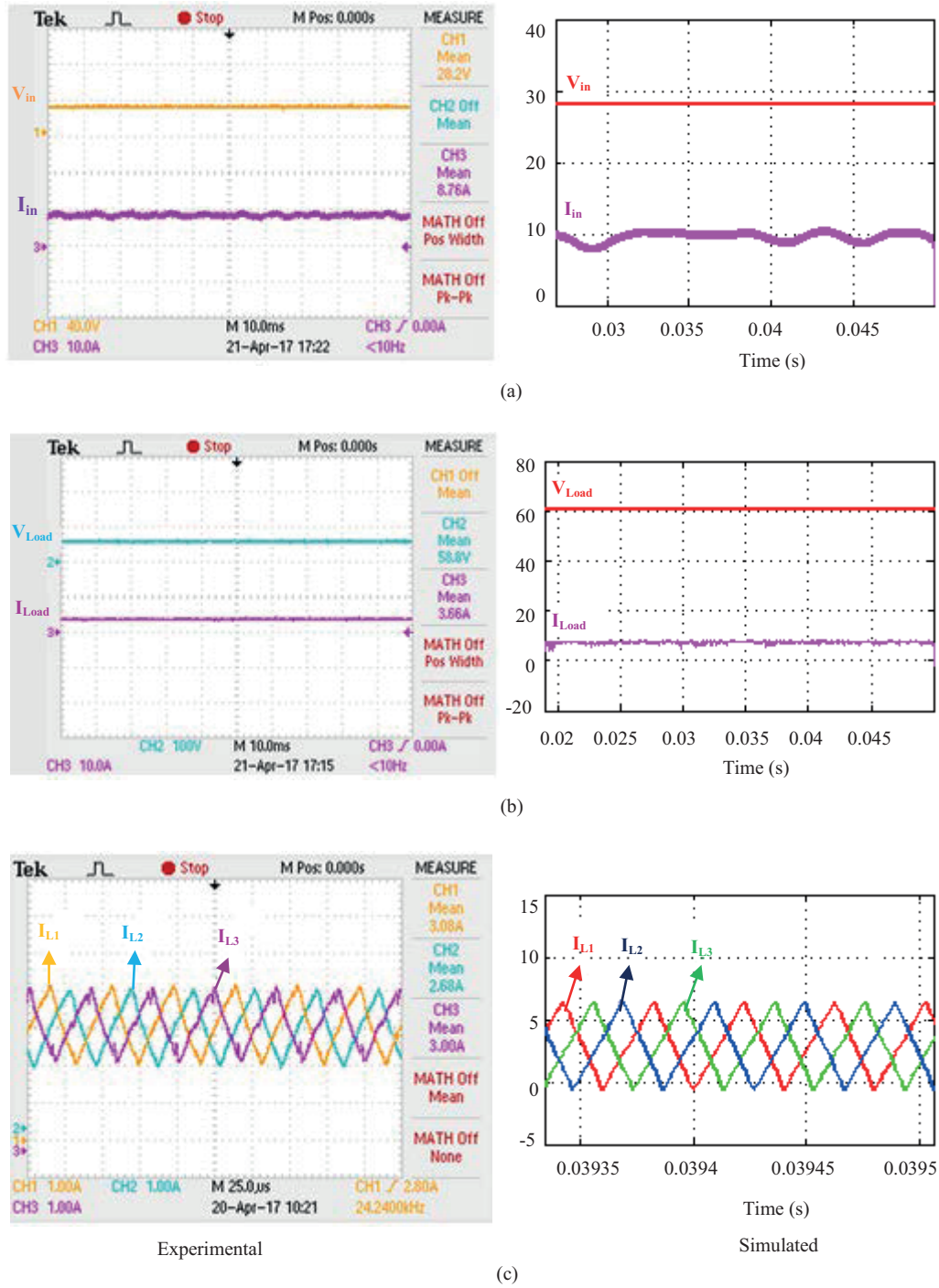

Figure 10. Characteristics of the proposed system with change in SOC of battery in buck mode.

Figure 11. Experimentation and simulation waveforms of BIDC in boost mode: (a) input voltage and current, (b) load voltage and current, (c) inductor currents.

During buck mode, the PV module is disconnected from the system by turning OFF switch S_1, which is reflected by the sudden change in PV module voltage and current. The PV module voltage, V_{OC}, is increased to its open circuit voltage, V_{OC}, of 37.25 V and the PV module current, I_{PV}, is reduced to zero as shown in

(a)

(b)

Experimental   Simulated

(c)
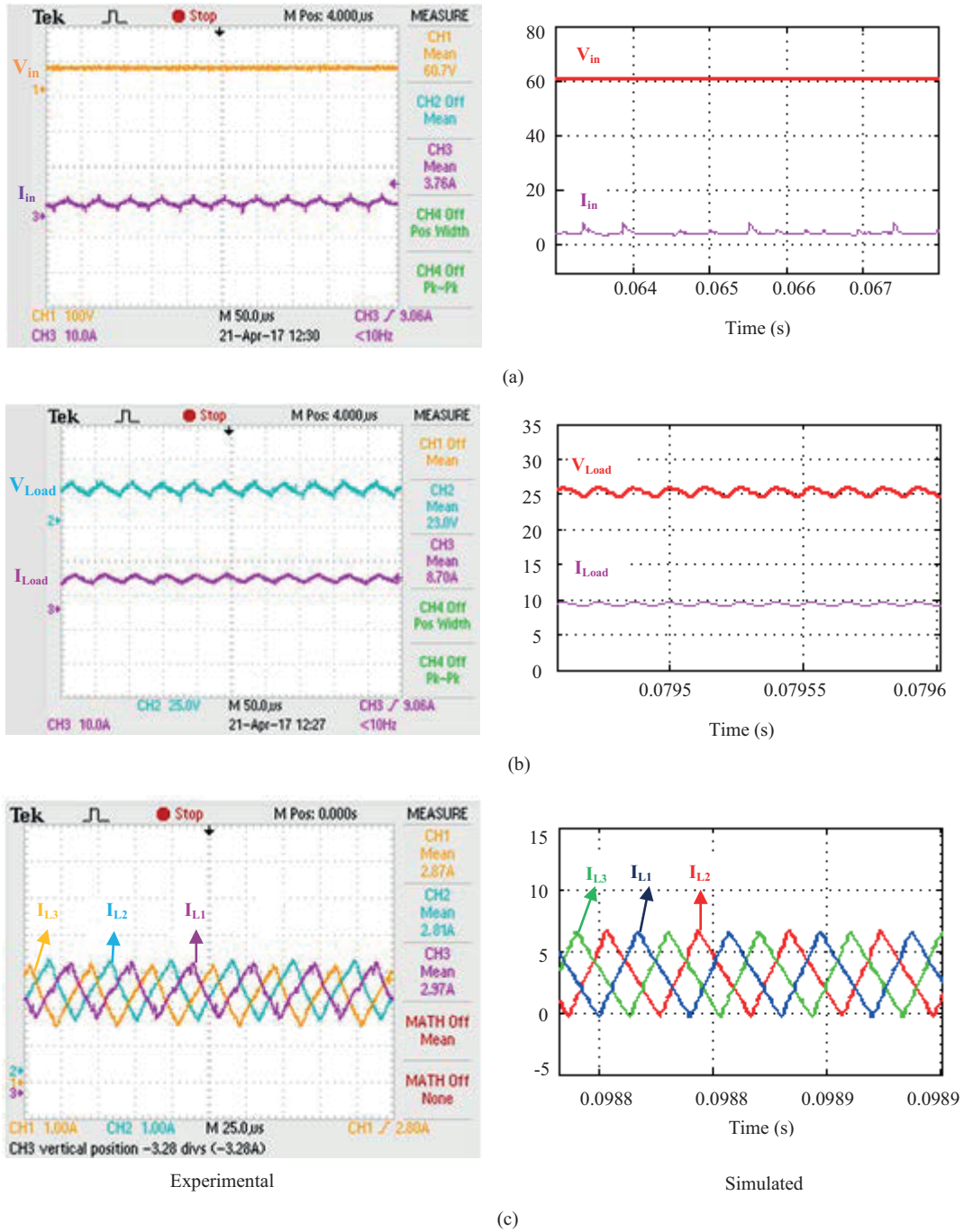
Figure 12. Experimentation and simulation waveforms of BIDC in buck mode: (a) input voltage and current, (b) load voltage and current, (c) inductor currents.

Figure 6a and Figure 6b, respectively. In this mode, as shown in Figure 6c, the EV battery discharges to drive the DC load, which is depicted by the positive battery current, I_{Batt}, as shown in Figure 6d. The DC load voltage, V_{Load}, and load current, I_{Load}, are increased to 25.26 V and 9.374 A respectively as shown in Figure 6e and Figure 6f, respectively. The inductor current waveforms in both modes of operation are shown in Figure7, which clearly indicates the reversal of flow of current in boost and buck mode. The zero voltage switching

waveforms of the BIDC in boost and buck mode shown in Figure 8 clearly depict that when the voltage across the switches, V_{CE}, is reduced to zero, the gate pulses are turned on.

The proposed system is simulated for various irradiation conditions during the charging (boost) mode and the corresponding BIDC output voltage to charge the EV battery and power fed to the EV battery are plotted in Figure 9. From Figure 9, it is evident that the power fed to the battery from the PV module is increasing with the increase in irradiation conditions and the battery is charged with a constant voltage of 60.5 V irrespective of the irradiation conditions. Also, the proposed system is simulated for various SOC conditions of the EV battery during discharging (buck) mode, and the corresponding power fed to the load and load voltage is plotted in Figure 10. Figure 10 shows that the power fed to the load is decreasing with the decrease in the SOC of the battery at a constant voltage fed to the load.

6. Experimental setup and results

The hardware prototype of the BIDC was fabricated and tested in the laboratory using the components specified in Table 2. A Magna programmable DC supply was used as the PV module emulator. The gate pulses were fed to the MOSFET switches of the BIDC using a PIC16F876A microcontroller and IR2130 driver circuit.

Table 2. Specifications of the proposed system.

Components	Specifications
Magna programmable DC supply	$0 - 125V, 0 - 48A$
MOSFET, IRF540	$100V, 28A$
Snubber capacitors	$0.1\mu F, 63V$
Inductors	$181\mu H, 15A$
Capacitor, C_L	$1\mu F, 450V$
Capacitor, C_H	$1500\mu F, 160V$
Resistive load	$50\Omega, 10A$

A 250-W BIDC prototype was tested separately in boost and buck modes and the results obtained in both simulation and experimentation are shown in this section. In boost mode, a conventional DC supply is connected on the low voltage side and the load is connected to the high voltage side of the BIDC. Gate pulses of frequency 25 kHz are provided to the switches of the BIDC with duty cycle of 0.56. The input voltage, V_{in}, of 28 V is boosted to 60 V and the input and output waveforms in boost mode are shown in Figure 11a and Figure 11b.

Also, the waveforms of the inductor currents, I_{L1}, I_{L2}, and I_{L3}, are shown in Figure 11c. In both simulation and experimentation, the efficiency of the BIDC was found to be approximately 90% at the power level of 250 W.

In buck mode, the DC supply is connected on the high voltage side and the load is connected to the low voltage side of the BIDC. The switches of the BIDC are provided with gate pulses of 25 kHz frequency with duty cycle of 0.42. The waveforms of experimentation and simulation results in buck mode are shown in Figure 12, which depicts that the input voltage, V_{in}, of 60 V is bucked to 25 V. In buck mode also, the efficiency is found to be approximately 90% at a power level of 200 W.

From the waveforms shown in Figures 11 and 12, it is evident that the experimentation results are in accordance with the simulation results, thus proving the efficacy of the system.

7. Conclusion

In this paper, an off-board EV battery charging system fed from a PV module using a BIDC is proposed for light-weight EVs. This paper discusses the flexibility of the system to charge the EV battery at standstill condition and also to operate the motor in running condition of the EV. The system is designed for 250 W and simulated in the MATLAB/Simulink environment, and the hardware prototype is fabricated and tested in the laboratory. Results are furnished for the two modes of operation of the proposed system. The characteristics of the proposed system are analyzed with different PV module irradiation conditions in forward (charging) mode and change in SOC of the battery in the reverse (discharging) mode in the simulation. The simulation and experimental results shown in Section 5 and Section 6 validate the working of the proposed system.

References

[1] Mekhilef S, Faramarzi SZ, Saidur R, Salam Z. The application of solar technologies for sustainable development of agricultural sector. Renewable & Sustainable Energy Reviews 2013; 18: 583–594.

[2] Krithiga S, Ammasai GN. Investigations of an improved PV system topology using multilevel boost converter and line commutated inverter with solutions to grid issues. Simulation Modelling Practice and Theory 2014; 42: 147–159.

[3] Badawy MO, Sozer Y. Power flow management of a grid tied PV-battery system for electric vehicles charging. IEEE Transactions on Industrial Applications 2017; 53: 1347–1357.

[4] Van DMD, Chandra MGR, Morales-Espana MG, Elizondo LR, Bauer P. Energy management system with PV power forecast to optimally charge EVs at the workplace. IEEE Transactions on Industrial Informatics 2018; 14: 311–320.

[5] Wirasingha SG, Emadi A. Pihef: Plug-in hybrid electric factor. IEEE Transactions on Vehicular Technology 2011; 60: 1279–1284.

[6] Huiling T, Jiekang W, Zhijiang W, Lingmin C. Two-stage optimization method for power loss and voltage profile control in distribution systems with DGs and EVs using stochastic second-order cone programming. Turkish Journal of Electrical Engineering & Computer Sciences 2018; 26: 501-517.

[7] Sushil KB, Krithiga S, Sarathi S P. Wireless electric vehicle battery charging system using PV array. Indian Journal of Science & Technology 2016; 9: 1-5.

[8] Khan IA. Battery chargers for electric and hybrid vehicles. In: IEEE 1994 Workshop on Power Electronics in Transportation; Dearborn, MI, USA; 1994. pp. 103–112.

[9] Farzin H, Fotuhi-Firuzabad M, Moeini-Aghtaie M. A practical scheme to involve degradation cost of lithium-ion batteries in vehicle-to-grid applications. IEEE Transactions on Sustainable Energy 2016; 7: 1730–1738.

[10] Chen X, Shen W, Vo TT, Cao Z, Kapoor A. An overview of lithium-ion batteries for electric vehicles. In: IEEE 2012 10th International Power Energy Conference; Ho Chi Minh City, Vietnam; 2012. pp. 230–235.

[11] Zubair R, Ibrahim A, Subhas M. Multiinput dc–dc converters in renewable energy applications – an overview. Renewable & Sustainable Energy Reviews 2015; 41: 521-539.

[12] Duong T, Sajib C, Yuanfeng L, Joeri VM, Omar H. Optimized multiport dc/dc converter for vehicle drive trains: topology and design optimization. Applied Science 2018; 1351: 1-17.

[13] Santhosh TK, Natarajan K, Govindaraju C. Synthesis and implementation of a multi-port dc/dc converter for hybrid electric vehicles. Journal of Power Electronics 2015; 15 (5): 1178-1189.

[14] Hongfei W, Peng X, Haibing H, Zihu Z, Yan X. Multiport converters based on integration of full-bridge and bidirectional dc–dc topologies for renewable generation systems. IEEE Transactions on Industrial Electronics 2014; 61: 856-869

[15] Jabbari M, Dorcheh MS. Resonant multi-input/multi-output/bidirectional ZCS step-down dc-dc converter with systematic synthesis for point-to-point power routing. IEEE Transactions on Power Electronics 2018; 33: 6024-6032.

[16] Neng Z, Danny S, Kashem MM. A review of topologies of three-port dc–dc converters for the integration of renewable energy and energy storage system. Renewable & Sustainable Energy Reviews 2016; 56: 388-401.

[17] Sujitha N, Krithiga S. RES based EV battery charging system: a review. Renewable & Sustainable Energy Reviews 2017; 75: 978–988.

[18] Inoue S, Akagi H. A bidirectional dc–dc converter for an energy storage system with galvanic isolation. IEEE Transactions on Power Electronics 2007; 22: 2299–2306.

[19] Farzad S, Seyed HH, Mehran S, Gevorg BG. Dynamic analysis of a modular isolated bidirectional dc-dc converter for high power applications. Turkish Journal of Electrical Engineering & Computer Sciences 2016; 24: 2174–2193.

[20] Xiaodong L, Hong-Yu L, Gao-Yuan H, Yu X. A bidirectional dual-bridge high-frequency isolated resonant DC/DC converter. In: IEEE 2013 8th Conference on Industrial Electronics & Applications; Melbourne, Australia; 2013. pp. 49–54.

[21] Du Y, Zhou X, Bai S, Lukic S, Huang A. Review of non-isolated bi-directional dc-dc converters for plug-in hybrid electric vehicle charge station application at municipal parking decks. In: IEEE 2010 Twenty-Fifth Annual IEEE Applications on Power Electronics; Palm Springs, CA, USA; 2010. pp. 1145–1151.

[22] Kwon M, Oh S, Choi S. High gain soft-switching bidirectional dc–dc converter for eco-friendly vehicles. IEEE Transactions on Power Electronics 2014; 29: 1659–1666.

[23] Mirzaei A, Jusoh A, Salam Z, Adib E, Farzanehfard H. Analysis and design of a high efficiency bidirectional dc–dc converter for battery and ultracapacitor applications. Simulation Modelling Practice & Theory 2011; 19: 1651–1667.

[24] Zhang J, Lai J S, Kim RY, Yu W. High-power density design of a soft-switching high-power bidirectional dc–dc Converter. IEEE Transactions on Power Electronics 2007; 22: 1145–1153.

[25] Junhong Z. Bidirectional dc-dc power converter design optimization, modeling and control. PhD, Virginia Polytechnic Institute, Blacksburg, VA, USA, 2008.

[26] Ji Tai H, Chang-Soon L, Ja-Hwi C, Kim R, Hyun D. A high efficiency non-isolated bidirectional dc-dc converter with zero-voltage-transition. In: IEEE 2013 39th Annual Conference on Industrial Electronics Society; Vienna, Austria; 2013. pp. 198–203.

[27] Henze CP, Martin HC, Parsley DW. Zero-voltage switching in high frequency power converters using pulse width modulation. In: IEEE 1988 Third Annual IEEE Applications on Power Electronics Conference & Expo; New Orleans, LA, USA; 1988. pp. 33–40.

[28] Krithiga S, Ammasai GN. Power electronic configuration for the operation of PV system in combined grid-connected and stand-alone modes. IET Power Electronics 2014; 7: 640–647.